INTERNATIONAL JOURNAL FOR NUMERICAL METHODS IN ENGINEERING, VOL. 39, 1199–1217 (1996)

SHAPE SENSITIVITY ANALYSIS FOR STEADY METAL-FORMING PROCESSES

ANTOINETTE M. MANIATTY AND MING-FA CHEN

Department of Mechanical Engineering, Aeronautical Engineering and Mechanics, Rensselaer Polytechnic Institute, Troy, NY 12180, U.S.A.

SUMMARY

This paper develops a numerical technique for determining the shape sensitivity parameters in steady metal-forming processes such as drawing and rolling. The adjoint method is applied to the discrete non-linear system of equations in the finite element model in order to determine the discrete matrix of sensitivity parameters. In this work, two specific cases are considered. The first case involves determining the sensitivity of the process power requirement to the process geometry and the second case involves determining the sensitivity of the internal state variable distribution in the final product to the process geometry. The process geometry is assumed to be characterized by a finite number of shape parameters. The internal state variable distribution in this case represents the resistance to plastic flow and is considered to be related to the quality of the final product. Numerical examples for a simple drawing process are presented to demonstrate the efficiency of the algorithm.

KEY WORDS: sensitivity analysis; shape optimization; extrusion; drawing

1. INTRODUCTION

Significant progress has been made in recent years in the numerical modelling of industrial forming processes using high-powered computing facilities.[1–4] These models are capable of handling the complicated large deformations, material constitutive laws and boundary conditions that arise in these processes. In the modelling of forming processes, generally a system of governing equations including the balance of linear momentum, kinematic equations and constitutive equations for the material are specified along with a description of the boundary conditions. Then a forward solution for the deformation, stress and state variable fields throughout the domain of interest is found. The computational modelling of these processes aids in the design by providing the capability to predict certain aspects of a process before actually building the physical facility to carry out the process.

These numerical models can also be used as bases for sensitivity analyses. In a sensitivity analysis, the effects of changes in process parameters on the final product or on other process variables are examined. Sensitivity analyses are used in the solution of inverse and optimization problems[5–9] and for control.[10–12] The most simple sensitivity analysis can be performed by simply solving the forward problem over the range of all possible combinations of process parameters and examining the results. This works well if there are few process parameters that can only vary over a very limited range, but becomes very inefficient if there are many process parameters or if the process parameters may be able to take on many different possible values since each solution of the forward problem is computationally intensive in itself. In these latter

CCC 0029–5981/96/071199–19

Received 5 February 1995
Revised 5 July 1995

cases, it is often desirable to find a matrix of sensitivity parameters which consists of derivatives of solution variables with respect to input variables that are computed for a given set of input variables. This would then provide a direction for updating the input variables in an inverse or optimization problem or for control purposes on-line. This matrix could be thought of as the coefficient matrix for the linearized problem.

This paper describes a method for determining matrices of discrete sensitivity parameters for steady metal-forming processes. The sensitivities that are investigated are shape sensitivities which are used to analyse the effect of the process geometry. Two specific cases will be investigated. The first case is to determine the effect of the process geometry on the power required for the process and the second case is to determine the effect of the process geometry on the state variables that define the state of the final product.

Significant effort has been devoted to non-linear sensitivity analysis in recent years. Tortorelli[13] compares the adjoint and direct differentiation methods used to formulate design sensitivities for non-linear constrained elastostatic systems. The problem of shape design sensitivity analysis for a variety of problems, both linear and non-linear, using the adjoint method is presented in Reference 14. Non-linear structural design sensitivity analysis involving inelastic material responses is presented in References 15 and 16. In metal-forming applications, Wenner[8] calculated the process sensitivities for sheet-metal forming by using a simple plane-strain approach in the problem formulation and Zhang *et al.*[17] determined the design sensitivity coefficients for finite deformation elasto-viscoplastic problems using the direct differentiation approach in a boundary element context. Michaleris *et al.*[18] compare the adjoint and direct differentiation methods used to formulate design sensitivities for steady and transient non-linear coupled problems with applications to elastoplasticity.

In this work, a procedure similar to that presented in Michaleris *et al.*[18] is used to determine discrete shape sensitivity parameters for steady metal-forming processes. Specifically, the adjoint method is used for deriving the sensitivity matrix for a coupled steady-state viscoplastic analysis. An augmented Lagrangian is formed for each case and differentiated to give the sensitivity coefficients in terms of adjoint state fields. The adjoint state fields that eliminate the implicit derivatives in the functional are determined. The discretized sensitivities can then be computed in an explicit matrix expression. The forward computational model that is used as a basis in this work is a coupled, Eulerian, viscoplastic finite element formulation following that given in Reference 1, but neglecting thermal effects. The elastic part is also neglected for simplicity and the deformation is assumed incompressible. A unified isotropic flow theory is used for the constitutive relations. The viscoplastic material behaviour is modeled using a scalar internal variable that represents the isotropic resistance to plastic flow. The model used herein is that given in Reference 19. Finally, an example involving a sheet-drawing process is used to investigate the efficiency and accuracy of the sensitivity analysis. The results are compared with that of a finite difference approach.

2. DISCRETIZATION OF THE STEADY FORMING PROBLEM

The formulation for the direct metal-forming problem follows that given in Reference 1. The notation used throughout is listed in Appendix III. Summarizing, consider a two-dimensional domain B with boundary ∂B where the material being deformed is flowing steadily through the domain. The boundary value problem for equilibrium on B is regarded as a control volume problem and is expressed in the following manner:

$$\operatorname{div} \mathbf{T} = \mathbf{0} \qquad \text{on } B$$

$$\mathbf{e}_i \cdot \mathbf{u} = \hat{u}_i \qquad \text{on } = \partial B_{1i} \quad i = 1, 2$$

$$\mathbf{e}_i \cdot (\mathbf{Tn}) = \hat{t}_i \qquad \text{on } \partial B_{2i} \qquad i = 1, 2$$

$$\mathbf{e}_i \cdot (\mathbf{Tn}) = \beta(u_{0i} - u_i) \quad \text{on } \partial B_{3i} \qquad i = 1, 2$$

where T is the Cauchy stress tensor, $\mathbf{u}$ is the velocity vector, $\hat{u}_i$ is the velocity specified on ∂B_{1i}, $\hat{t}_i$ is the traction specified on ∂B_{2i}, $\mathbf{n}$ is the unit outward normal vector on ∂B and $\mathbf{e}_i$ form an orthonormal basis for the two-dimensional space with $i = 1, 2$. Furthermore, the fourth equation represents a hydrodynamic friction law where u_{0i} is the tangential velocity of the tool on ∂B_{3i} and β is the coefficient of hydrodynamic friction. In general, β is a function of the temperature and the normal traction, but in this analysis, it will be taken as constant for simplicity. The boundary conditions must be specified on the entire boundary for each degree of freedom without overlap, so $\partial B_{1i} \cup \partial B_{2i} \cup \partial B_{3i} = \partial B$ and $\partial B_{ji} \cap \partial B_{ki} = \phi$ for $i = 1, 2$ and $j \neq k$.

In this analysis, elasticity will be neglected for simplicity. Furthermore, the deformation is assumed to be isochoric which is typical for metal plasticity. Therefore,

$$\text{tr}(\mathbf{D}) = \text{div}\, \mathbf{u} = 0$$

where $\mathbf{D} = \text{sym}(\nabla \mathbf{u})$ is the rate of deformation tensor. The material is modelled by a unified isotropic viscoplastic flow theory, where an internal state variable represents the first-order resistance to deformation, such that

$$\dot{\varepsilon} = f(\sigma, s) \quad \mathbf{T}' = 2\mu_e \mathbf{D}$$

where

$$\dot{\varepsilon} = \sqrt{\tfrac{2}{3}\mathbf{D} \cdot \mathbf{D}} \quad \sigma = \sqrt{\tfrac{3}{2}\mathbf{T}' \cdot \mathbf{T}'}$$

$$\mathbf{T}' = \mathbf{T} - \tfrac{1}{3}(\text{tr}\, \mathbf{T})\mathbf{I} = \mathbf{T} + p\mathbf{I}$$

Here s is a scalar internal variable which is related to the strength of the material and p is the pressure. Note that from the above equations the effective viscosity is $\mu_e = \sigma/3\dot{\varepsilon}$.

In forming the finite element model, the equilibrium equation is converted to a weak form by applying the divergence theorem and substituting in the constitutive relations. The stress is decomposed into deviatoric and pressure components, with the pressure being indeterminate from the kinematics due to incompressibility. The assumption of incompressible deformation defines a constraint equation on the solution of the velocity field. This forms the second variational equation. These two equations can be put into matrix form by discretizing the domain and defining finite element interpolations for the velocity and pressure fields. The incompressibility constraint is known to sometimes cause ill-conditioning which causes spurious pressure modes. Several techniques have been proposed to avoid such behaviour.[20–25]. The consistent penalty method is shown to be acceptably accurate and efficient for incompressible media,[20] and therefore is applied in this study. In this work, a discontinuous pressure field is used which allows the nodal pressures to be expressed easily in terms of the nodal velocities and eliminated from the system of equations. So the system is reduced to a non-linear system of equations of the matrix form (see Appendix I for details)

$$\bar{\mathbf{k}}(\bar{\mathbf{u}}, \bar{\mathbf{s}}) = \bar{\mathbf{f}} \tag{1}$$

where $\bar{\mathbf{u}}$ and $\bar{\mathbf{s}}$ are vectors of the nodal velocities and state variables, respectively, and $\bar{\mathbf{f}}$ is the force vector.

In addition, an evolution equation for the state variable s is required to describe the evolution of the material state that arises during deformation. This can be expressed as

$$\dot{s} = g(\dot{\varepsilon}, s)$$

where overdot denotes a material time derivative and $\dot{\varepsilon}$ is the effective rate of deformation. Since steady problems are being considered, $\dot{s} = \nabla s \cdot \mathbf{u}$. Now a boundary value problem for the state variable can be expressed as

$$\nabla s \cdot \mathbf{u} = g(\dot{\varepsilon}, s) \quad \text{on } B$$

$$s = \hat{s} \quad \text{on } \partial B_s$$

where $\hat{s}$ is the initial value of the state variable on the entrance boundary ∂B_s.

Converting this to a variational form and substituting in finite element interpolating functions for the velocity and state variable fields gives a non-linear system of equations of the matrix form (see Appendix I for details)

$$\bar{\mathbf{h}}(\bar{\mathbf{u}}, \bar{\mathbf{s}}) = \mathbf{0} \tag{2}$$

Equations (1) and (2) are a coupled system of non-linear equations for nodal velocities $\bar{\mathbf{u}}$ and nodal state variables $\bar{\mathbf{s}}$. A staggered procedure has been found to work well for solving this system. The basic algorithm is described as follows:

(i) Guess $\bar{\mathbf{u}}$ and $\bar{\mathbf{s}}$, and keeping $\bar{\mathbf{s}}$ constant solve equation (1) for $\bar{\mathbf{u}}$ by the successive-substitution approach until within the radius of convergence and then finish solving with a Newton–Raphson method combined with a line search scheme.
(ii) Holding $\bar{\mathbf{u}}$ constant, solve equation (2) by the Newton–Raphson method for $\bar{\mathbf{s}}$.
(iii) Check global convergence criteria (both $\bar{\mathbf{u}}$ and $\bar{\mathbf{s}}$ satisfy equations (1) and (2) to within some tolerance), if not, go back to step (i) using the updated values of $\bar{\mathbf{u}}$ and $\bar{\mathbf{s}}$ as the new guess.

3. MATRIX FORMULATION OF SHAPE SENSITIVITY PARAMETERS

The shape sensitivity problem can be defined in terms of the forward analysis. In this case, the same governing equations and boundary conditions are prescribed, but now part of the boundary $\partial\hat{B}$ which represents the process geometry is variable. The shape of $\partial\hat{B}$ can defined by a position vector $\hat{\mathbf{x}}(\xi)$ which can be parameterized by

$$\mathbf{e}_i \cdot \hat{\mathbf{x}}(\xi) = \bar{b}_{i\alpha}\varphi_\alpha(\xi), \quad \hat{\mathbf{x}} \in \partial\hat{B}, \quad i = 1, 2, \quad \alpha = 1, N_{\mathcal{B}} \tag{3}$$

where $\bar{b}_{i\alpha}$ (or $\bar{\mathbf{b}}$ in direct notation) are the shape design parameters, φ_α are shape functions, ξ is a measure of distance along $\partial\hat{B}$, and $N_{\mathcal{B}}$ is the number of discrete points used to parameterize the boundary $\partial\hat{B}$. Summation is assumed on the repeated index α. Now the non-linear system of governing equations (1) and (2) becomes

$$\bar{\mathbf{k}}(\bar{\mathbf{u}}, \bar{\mathbf{s}}, \bar{\mathbf{b}}) = \bar{\mathbf{f}}(\bar{\mathbf{b}}) \tag{4}$$

$$\bar{\mathbf{h}}(\bar{\mathbf{u}}, \bar{\mathbf{s}}, \bar{\mathbf{b}}) = \mathbf{0} \tag{5}$$

where $\bar{\mathbf{b}}$ is added to the list of variables. It should be noted that in many cases only one component of the position vector $\hat{\mathbf{x}}(\xi)$ will be variable, i.e. $i = 1$ or 2. So to be more general, let N_d be the total number of shape design variables.

3.1. Case 1: Shape sensitivities of power requirement

Let the process be driven by the tool contacting the workpiece on part of the boundary $\partial B'$. In the case of drawing, $\partial B'$ would be the exit region where the tool pulls the workpiece through the die and in rolling, it would be the roll–workpiece interface, for example. The power required to drive the process is

$$P = \int_{\partial B'} \mathbf{t} \cdot \mathbf{u}' \, dA$$

where P denotes power, $\mathbf{t}$ is the traction vector and $\mathbf{u}'$ is the tool velocity on $\partial B'$. Generally, the tool velocity on $\partial B'$ is a constant over the contact area. For example in rolling, it is just the roll surface velocity, and in drawing, it is the exit velocity with which the workpiece is being pulled. Therefore, the above equation can be simplified using the finite element discretization as

$$P = \left[\int_{\partial B'} \mathbf{t} \, dA \right] \cdot \mathbf{u}' = \bar{\mathbf{f}}'^{\mathrm{T}} \bar{\mathbf{u}}'$$

where $\bar{\mathbf{f}}'$ and $\bar{\mathbf{u}}'$ are the vectors of nodal forces and velocities on $\partial B'$. The shape sensitivity parameters for the power are then

$$\frac{dP}{d\bar{\mathbf{b}}} = \left[\frac{d\bar{\mathbf{f}}'}{d\bar{\mathbf{b}}} \right]^{\mathrm{T}} \bar{\mathbf{u}}' = \mathbf{B}^{\mathrm{T}} \bar{\mathbf{u}}' \tag{6}$$

where $\bar{\mathbf{u}}'$ is assumed to be held fixed to give the desired process speed and $\mathbf{B} = [d\bar{\mathbf{f}}'/d\bar{\mathbf{b}}]$. Therefore, the matrix of shape sensitivity parameters of interest is $\mathbf{B}$ since $\bar{\mathbf{u}}'$ is assumed to be prescribed.

The shape sensitivity parameters $\mathbf{B}$ can be computed using a finite difference approximation of

$$\lim_{\Delta\bar{\mathbf{b}} \to \mathbf{0}} (\mathbf{B}\Delta\bar{\mathbf{b}} = \bar{\mathbf{f}}'(\bar{\mathbf{t}}', \bar{\mathbf{b}} + \Delta\bar{\mathbf{b}}) - \bar{\mathbf{f}}'(\bar{\mathbf{t}}', \bar{\mathbf{b}})) \tag{7}$$

where $\bar{\mathbf{f}}'$ is found by solving the forward problem in each case and the tractions $\bar{\mathbf{t}}'$ depend implicitly on the shape parameters $\bar{\mathbf{b}}$. For problems where there are a large number of design parameters, i.e. N_d is not small, this problem requires a large number of computations since the forward problem needs to be solved $N_d + 1$ times to determine $\mathbf{B}$. Therefore, an alternative approach requiring less computations is desirable.

Since the tractions on $\partial B'$ depend on the shape parameters $\bar{\mathbf{b}}$, these tractions can be considered as unknowns. If no boundary condition is prescribed on $\partial B'$, equation (4) becomes

$$\bar{\mathbf{k}}^*(\bar{\mathbf{u}}, \bar{\mathbf{s}}, \bar{\mathbf{b}}) = \bar{\mathbf{f}}^*(\bar{\mathbf{t}}, \bar{\mathbf{b}}) = \bar{\mathbf{f}}_1^*(\hat{\bar{\mathbf{t}}}, \bar{\mathbf{b}}) + \bar{\mathbf{f}}_2^*(\bar{\mathbf{t}}', \bar{\mathbf{b}}) \tag{8}$$

with

$$\bar{\mathbf{t}} = \hat{\bar{\mathbf{t}}} + \bar{\mathbf{t}}'$$

where $\hat{\bar{\mathbf{t}}}$ is the vector of nodal tractions prescribed on ∂B_{2t}, $\bar{\mathbf{t}}'$ is the vector of unknown nodal tractions on $\partial B'$ and the asterisk denotes that this is a different system from that in equation (4). The part of the force vector due to the unknown tractions on $\partial B'$ is the part of interest. Therefore, defining a rectangular matrix $\mathbf{Q}$ such that $\mathbf{Q}\bar{\mathbf{f}}_1^*(\hat{\bar{\mathbf{t}}}, \bar{\mathbf{b}}) = \mathbf{0}$ and $\mathbf{Q}\bar{\mathbf{f}}_2^*(\bar{\mathbf{t}}, \bar{\mathbf{b}}) = \bar{\mathbf{f}}'(\bar{\mathbf{t}}, \bar{\mathbf{b}})$ gives

$$\mathbf{Q}\bar{\mathbf{k}}^*(\bar{\mathbf{u}}, \bar{\mathbf{s}}, \bar{\mathbf{b}}) = \bar{\mathbf{f}}'(\bar{\mathbf{t}}', \bar{\mathbf{b}}) \tag{9}$$

where $\bar{\mathbf{f}}'(\bar{\mathbf{t}}, \bar{\mathbf{b}})$ is the subvector of the force vector $\bar{\mathbf{f}}^*(\bar{\mathbf{t}}, \bar{\mathbf{b}})$ which contains only the elements which depend on $\bar{\mathbf{t}}'$. Now the sensitivity coefficient matrix $\mathbf{B}$ can be defined as

$$\mathbf{B} = \frac{d\bar{\mathbf{f}}'}{d\bar{\mathbf{b}}} = \frac{\partial \bar{\mathbf{f}}'}{\partial \bar{\mathbf{t}}'} \frac{d\bar{\mathbf{t}}'}{d\bar{\mathbf{b}}} + \frac{\partial \bar{\mathbf{f}}'}{\partial \bar{\mathbf{b}}} = \mathbf{Q}\left[\frac{\partial \bar{\mathbf{k}}^*}{\partial \bar{\mathbf{u}}} \frac{d\bar{\mathbf{u}}}{d\bar{\mathbf{b}}} + \frac{\partial \bar{\mathbf{k}}^*}{\partial \bar{\mathbf{s}}} \frac{d\bar{\mathbf{s}}}{d\bar{\mathbf{b}}} + \frac{d\bar{\mathbf{k}}^*}{d\bar{\mathbf{b}}}\right] \tag{10}$$

While the matrices $[\partial \bar{\mathbf{k}}^*/\partial \bar{\mathbf{u}}]$, $[\partial \bar{\mathbf{k}}^*/\partial \bar{\mathbf{s}}]$, $[\partial \bar{\mathbf{k}}^*/\partial \bar{\mathbf{b}}]$ and $[\partial \bar{\mathbf{f}}'/\partial \bar{\mathbf{b}}]$ are explicit derivatives and can be computed readily, the matrices $[\partial \bar{\mathbf{u}}^*/\partial \bar{\mathbf{b}}]$, $[\partial \bar{\mathbf{s}}/\partial \bar{\mathbf{b}}]$ and $[\partial \bar{\mathbf{t}}'/\partial \bar{\mathbf{b}}]$ are implicit derivatives which cannot be computed directly. The adjoint method can be used to eliminate these implicit derivatives so that the shape sensitivities $\mathbf{B}$ can be determined directly.

In the adjoint method, an augmented Lagrangian is defined in terms of adjoint variable fields. The adjoint variable fields are then defined so as to eliminate the implicit derivatives. Following the method of Arora and Cardoso,[14] let $\bar{q}_I$ represent the general functions for which the sensitivities are to be determined. In this case, $\bar{q}_I$ is defined as

$$\bar{q}_I(\bar{\mathbf{u}}, \bar{\mathbf{s}}, \bar{\mathbf{b}}) = \tilde{f}'_I(\bar{\mathbf{t}}', \bar{\mathbf{b}}) = Q_{IJ} \bar{k}^*_J(\bar{\mathbf{u}}, \bar{\mathbf{s}}, \bar{\mathbf{b}}), \quad I = 1, 2N_{B'}, \; J = 1, 2N \tag{11}$$

where $N_{B'}$ is the number of nodes on the boundary with the unknown tractions which are to be minimized, i.e. $\partial B'$, N is the total number of nodes for the velocity interpolation and summation is assumed on index J. The state equations are equations (4) and (5) where a velocity or friction boundary condition is prescribed on $\partial B'$ which represents the desired process speed for which the shape sensitivities are being determined. Then the augmented functional can be expressed as

$$L(\bar{\mathbf{u}}, \bar{\mathbf{u}}^a, \bar{\mathbf{s}}, \bar{\mathbf{s}}^a, \bar{\mathbf{b}}) = \bar{q}_I(\bar{\mathbf{u}}, \bar{\mathbf{s}}, \bar{\mathbf{b}}) + W^a_1(\bar{\mathbf{u}}, \bar{\mathbf{s}}, \bar{\mathbf{b}}, \bar{\mathbf{u}}^a) + W^a_2(\bar{\mathbf{u}}, \bar{\mathbf{s}}, \bar{\mathbf{b}}, \bar{\mathbf{s}}^a) \tag{12}$$

where

$$W^a_1(\bar{\mathbf{u}}, \bar{\mathbf{s}}, \bar{\mathbf{b}}, \bar{\mathbf{u}}^a) = \bar{\mathbf{u}}^{aT}[\bar{\mathbf{f}}(\bar{\mathbf{b}}) - \bar{\mathbf{k}}(\bar{\mathbf{u}}, \bar{\mathbf{s}}, \bar{\mathbf{b}})] \tag{13}$$

$$W^a_2(\bar{\mathbf{u}}, \bar{\mathbf{s}}, \bar{\mathbf{b}}, \bar{\mathbf{s}}^a) = \bar{\mathbf{s}}^{aT}[\bar{\mathbf{h}}(\bar{\mathbf{u}}, \bar{\mathbf{s}}, \bar{\mathbf{b}})] \tag{14}$$

and where $\bar{\mathbf{u}}^a$ and $\bar{\mathbf{s}}^a$ are admissible adjoint fields which are to be determined. The adjoint fields are found by specifying

$$\frac{\partial L}{\partial \bar{\mathbf{u}}} = \mathbf{0} \quad \text{and} \quad \frac{\partial L}{\partial \bar{\mathbf{s}}} = \mathbf{0} \tag{15}$$

and solving simultaneously for $\bar{\mathbf{u}}^a$ and $\bar{\mathbf{s}}^a$. Then the sensitivity parameters can be determined from

$$\frac{d\bar{q}_I}{d\bar{\mathbf{b}}} = \frac{\partial L}{\partial \bar{\mathbf{b}}} \tag{16}$$

thus reducing a total derivative to a partial derivative. Evaluating these equations gives

$$\mathbf{B} = \frac{d\bar{\mathbf{q}}}{d\bar{\mathbf{b}}} = \mathbf{K}^*_b + \mathbf{K}^*_u(\mathbf{K}_u - \mathbf{K}_s\mathbf{H}_s^{-1}\mathbf{H}_u)^{-1}(\mathbf{F}_b - \mathbf{K}_b) + \mathbf{K}^*_s(\mathbf{K}_s - \mathbf{K}_u\mathbf{H}_u^{-1}\mathbf{H}_s)^{-1}(\mathbf{F}_b - \mathbf{K}_b)$$

$$+ \mathbf{K}^*_u(\mathbf{H}_s\mathbf{K}_s^{-1}\mathbf{K}_u - \mathbf{H}_u)^{-1}\mathbf{H}_b + \mathbf{K}^*_s(\mathbf{K}_u\mathbf{K}_u^{-1}\mathbf{K}_s - \mathbf{K}_s)^{-1}\mathbf{H}_b \tag{17}$$

where

$$\mathbf{K}_b^* = \mathbf{Q}\frac{\partial \bar{\mathbf{k}}^*}{\partial \bar{\mathbf{b}}} \quad \mathbf{K}_u^* = \mathbf{Q}\frac{\partial \bar{\mathbf{k}}^*}{\partial \bar{\mathbf{u}}}, \quad \mathbf{K}_s^* = \mathbf{Q}\frac{\partial \bar{\mathbf{k}}^*}{\mathrm{d}\bar{\mathbf{s}}}$$

$$\mathbf{K}_b = \frac{\partial \bar{\mathbf{k}}}{\partial \bar{\mathbf{b}}}, \qquad \mathbf{K}_u = \frac{\partial \bar{\mathbf{k}}}{\partial \bar{\mathbf{u}}}, \qquad \mathbf{K}_s = \frac{\partial \bar{\mathbf{k}}}{\partial \bar{\mathbf{s}}}, \quad \mathbf{F}_b = \frac{\partial \bar{\mathbf{f}}}{\partial \bar{\mathbf{b}}}$$

$$\mathbf{H}_b = \frac{\partial \bar{\mathbf{h}}}{\partial \bar{\mathbf{b}}}, \qquad \mathbf{H}_u = \frac{\partial \bar{\mathbf{h}}}{\mathrm{d}\bar{\mathbf{u}}}, \qquad \mathbf{H}_s = \frac{\partial \bar{\mathbf{h}}}{\partial \bar{\mathbf{s}}}$$

The vector $\bar{\mathbf{q}}$ consists of the elements $\bar{q}_I$ where $I = 1, 2N_{B'}$. The matrices $\mathbf{K}_u$ and $\mathbf{H}_s$ are the tangent matrices used in the Newton–Raphson solution of the forward problem and would therefore normally already be computed. The matrices $\mathbf{K}_s$ **and** $\mathbf{H}_u$ are also tangent matrices which can be computed directly. The matrices $\mathbf{K}_b$, $\mathbf{F}_b$ and $\mathbf{H}_b$ can be found efficiently using a finite difference approximation. It should be noted that this is different and more efficient than the computation required in equation (7) because these are partial rather than total derivatives. Whereas the calculation indicated in equation (7) requires solving the forward problem $N_d + 1$ times, the matrices $\mathbf{K}_b$, $\mathbf{F}_b$ and $\mathbf{H}_b$ only require evaluating the vectors $\bar{\mathbf{k}}$, $\bar{\mathbf{f}}$ and $\bar{\mathbf{h}}$ $N_d + 1$ times holding $\bar{\mathbf{u}}$, $\bar{\mathbf{s}}$, and $\bar{\mathbf{t}}'$ fixed. Finally, the matrices $\mathbf{K}_b^*$, $\mathbf{K}_u^*$ and $\mathbf{K}_s^*$ are just submatrices of $\mathbf{K}_b$, $\mathbf{K}_u$ and $\mathbf{K}_s$ with modifications only in the rows and columns where the boundary conditions are different. Details for the calculation of $\mathbf{K}_u$, $\mathbf{K}_s$, $\mathbf{H}_s$ and $\mathbf{H}_u$ are given in Appendix II. This procedure is sometimes referred to as the semi-analytical method of sensitivity analysis.[26]

3.2. Case 2. Shape sensitivities of state variables

The adjoint method is also used to determine the sensitivity of the state variables in the final product with respect to the geometric parameters. The method follows that used in the previous section. In this case, the sensitivity parameters of interest are

$$\mathbf{C} = \frac{\mathrm{d}\bar{\mathbf{s}}'}{\mathrm{d}\bar{\mathbf{b}}}$$

where $\bar{\mathbf{s}}'$ is the vector of nodal state variables on the boundary in the exit zone ∂B_e. Since $\bar{\mathbf{s}}'$ is a subvector of $\bar{\mathbf{s}}$, a rectangular matrix $\mathbf{R}$ can be defined such that $\bar{\mathbf{s}}' = \mathbf{R}\bar{\mathbf{s}}$.

As in the previous case, the adjoint method can be used to determine the design sensitivity matrix. In this case, the general functions for which the sensitivities are to be determined are

$$\bar{r}_I(\bar{\mathbf{s}}) = \bar{s}'_I = R_{IJ}\bar{s}_J, \quad I = 1, N_{B_e}, \; J = 1, N$$

where N_{B_e} is the number of nodes on the exit boundary ∂B_e. The state equations are exactly the same as in the previous example with $\bar{r}_I$ in place of $\bar{q}_I$. So the augmented Lagrangian is

$$\tilde{L}(\bar{\mathbf{u}}, \bar{\mathbf{u}}^a, \bar{\mathbf{s}}, \bar{\mathbf{s}}^a, \bar{\mathbf{b}}) = \bar{r}_I(\bar{\mathbf{s}}) + W_1^a(\bar{\mathbf{u}}, \bar{\mathbf{s}}, \bar{\mathbf{b}}, \bar{\mathbf{u}}^a) + W_2^a(\bar{\mathbf{u}}, \bar{\mathbf{s}}, \bar{\mathbf{b}}, \bar{\mathbf{s}}^a)$$

where W_1^a and W_2^a are defined in equations (13) and (14). As before, $\bar{\mathbf{u}}^a$ and $\bar{\mathbf{s}}^a$ are found by satisfying equations (15), but now replacing the augmented Lagrangian L with $\tilde{L}$. Then the

sensitivity parameters can be determined using an equation analogous to equation (16):

$$\mathbf{C} = \frac{\mathrm{d}\bar{\mathbf{r}}}{\mathrm{d}\mathbf{b}} = \mathbf{R}[(\mathbf{K}_s - \mathbf{K}_u\mathbf{H}_u^{-1}\mathbf{H}_s)^{-1}(\mathbf{F}_b - \mathbf{K}_b) + (\mathbf{H}_u\mathbf{K}_u^{-1}\mathbf{K}_s - \mathbf{H}_s)^{-1}\mathbf{H}_b] \tag{18}$$

where $\bar{\mathbf{r}}$ is the vector of the elements r_I where $I = 1, N_{B_e}$; the matrices $\mathbf{K}_u$, $\mathbf{K}_s$, $\mathbf{H}_u$, $\mathbf{H}_s$, $\mathbf{K}_b$ and $\mathbf{F}_b$ and $\mathbf{H}_b$ are the same as defined in the previous section.

The procedure to calculate the sensitivity matrices **B** and **C** in equations (17) and (18) is briefly described as follows:

(1) Solve the forward problem and store $\bar{\mathbf{u}}$, $\bar{\mathbf{s}}$, $\bar{\mathbf{k}}$, $\bar{\mathbf{h}}$, $\bar{\mathbf{f}}$, $\mathbf{K}_u$ and $\mathbf{H}_s$.
(2) Compute $\bar{\mathbf{K}}_s$ and $\bar{\mathbf{H}}_u$.
(3) Perturb a design variable $\bar{b}_{i\alpha}$ by a the small value Δb and calculate the following vectors without solving the system equations:

   (i) $\bar{\mathbf{k}}$, $\bar{\mathbf{h}}$ and $\bar{\mathbf{f}}$ with applied velocity boundary conditions on $\partial B'$.
   (ii) $\mathbf{Q}\bar{\mathbf{k}}^*$ without applied velocity boundary conditions on $\partial B'$.

(4) Use the vectors computed in (1) and (3) to determine the corresponding components of the matrices $\mathbf{K}_b$, $\mathbf{F}_b$, $\mathbf{H}_b$ and $\mathbf{K}_b^*$ using a finite difference approximation and repeat procedure (2) until all design variables are perturbed and all the elements of the matrices defined.
(5) Extract the equivalent components of the matrices $\mathbf{K}_u^*$ and $\mathbf{K}_s^*$ from $\mathbf{K}_u$ and $\mathbf{K}_s$ and compute the remaining components associated with unknown boundary conditions on $\partial B'$.
(6) Calculate the sensitivity matrices using equations (17) and (18).

4. NUMERICAL EXAMPLES AND DISCUSSION

A series of numerical experiments are presented to demonstrate the level of computational accuracy and to show the results for the sensitivity parameters. A simple example of a steady metal-forming process, plane-strain hot drawing, is used in this study. In the first numerical experiment, the solution of the forward problem is analysed to investigate the accuracy and the effect of the penalty parameter on the solution. Also, the effect of the die shape on the power and on the state variable field is demonstrated. In the second and third numerical experiments, the sensitivity matrices **B** and **C** as defined in Sections 3.1 and 3.2, respectively, are computed and the results are compared to those obtained using a finite difference approach. The geometry and the boundary conditions of the workpiece for the drawing problem used in each example are shown in Figure 1, where $\partial\tilde{B} = \partial B_{1y} + \partial B_{2x}$; $\partial B' = \partial B_{1x} + \partial B_{2y}$; $\partial B^f = \partial B_{2x} + \partial B_{2y}$; and $\partial\hat{B} = \partial B_{3x'} + \partial B_{1y'}$. Symmetry is assumed about the centerline at $y = 0$. The co-ordinates x' and y' are tangent and normal co-ordinates on $\partial\hat{B}$, respectively. Specifically, on surface $\partial\tilde{B}$ the velocity is constrained to be in the horizontal direction with no friction; on surface $\partial B'$ the drawing speed is applied in the horizontal direction; surfaces ∂B^f are free surfaces; and on surface $\partial\hat{B}$ the normal velocity is zero and a friction condition is applied in the tangential direction. The domain of interest is divided into 36 eight-node elements for a total of 169 nodes for the velocity field interpolation. The pressure field is interpolated with three-node discontinuous pressure elements. Although this mesh is quite coarse, it was found to give reasonable accuracy and is useful for demonstrating the algorithm. The constitutive model presented in Reference 19 is assumed and is given in Table I. The material in these examples is taken to be 1100 Aluminum at 450°C and its material parameters are listed in Table II. The parameter s_0 is the initial value of s.

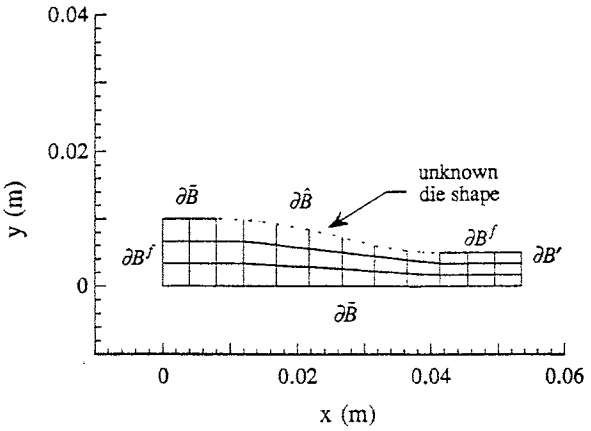

Figure 1. Geometry and boundary conditions for the sample drawing problem

Table I. Constitutive equations

Flow equations:	$\dot{\varepsilon} = \bar{A}\left[\sinh\left(\xi\frac{\sigma}{s}\right)\right]^{1/m}$,
Evolution equation:	$\dot{s} = \left[h_0\left\lvert 1 - \frac{s}{s^*}\right\rvert^a \operatorname{sign}\left(1 - \frac{s}{s^*}\right)\right]\dot{\varepsilon}$
where	$\bar{A} = A\exp\left(-\frac{Q}{R\theta}\right)$
	$s^* = \tilde{s}^*\left[\frac{\dot{\varepsilon}}{\bar{A}}\right]^n$
	R = gas constant, θ = absolute temperature A, Q, ξ, m, h_0, a, $\tilde{s}$ and n are material parameters.

Table II. Material parameters for 1100 Al at 450°C

s_0	29·5 MPa
$\bar{A}$	$4{\cdot}13 \times 10^{-6}$ sec^{-1}
ξ	7·00
m	0·23348
$\tilde{s}$	18·9 MPa
n	0·07049
h_0	1115·6 MPa
a	1·3

4.1. Experiment I: Forward problem

The accuracy of the sensitivity parameters will depend on the accuracy of the solution to the forward problem about which the sensitivity parameters are being determined. Therefore, the first numerical experiment is with regards to numerical accuracy of the forward problem. The

forward-problem solution is also useful for demonstrating the effect of the process parameters on the solution for specific cases as will be shown.

The penalty parameter in the consistent penalty method used to impose the incompressibility constraint is known to affect the accuracy and stability of the solution in the viscoplastic problem. This numerical behaviour can have a large effect on the sensitivity analysis. So it is important to choose a valid penalty parameter that gives a stable and accurate solution. In the following examples, the friction factor is taken as $\beta = 10^8$ Pa s m^{-1}. The reduction of the drawing process is 50 per cent as shown in Figure 1 and the drawing speed of the workpiece is 0·005 m/sec. In Figure 2, it is shown that the penalty parameter does not affect the results for the velocities much when the penalty parameter λ_p used is in the range of 10^{10}–10^{15}. In this range, the incompressibility constraint was found to be satisfied well too. In Figure 3, the residual for equation (1) is plotted as a function of the penalty parameter. To be specific, this residual is defined as

$$R = (\bar{\mathbf{k}}(\bar{\mathbf{u}}, \bar{\mathbf{s}}) - \bar{\mathbf{f}})^{\mathrm{T}}(\bar{\mathbf{k}}(\bar{\mathbf{u}}, \bar{\mathbf{s}}) - \bar{\mathbf{f}})$$

The accuracy of the finite difference approximation used in determining the sensitivity parameters decreases as the residual function increases. The upper limit for acceptable accuracy in the finite difference approach is shown. This is based on the size of the elements of $\Delta\mathbf{b}$ used in the finite difference approximations which are of the order 10^{-6} m. To maintain accuracy, the upper limit for the penalty parameter is therefore 10^{11}. Therefore, the penalty parameter that is taken for the problems herein is $\lambda_p = 10^{11}$. This is about four orders of magnitude higher than the typical pressure.

The solution for the case with the penalty parameter $\lambda_p = 10^{11}$ is now examined. Since the reduction is 50 per cent, and the drawing speed is 0·005 m/sec, the entering speed of the plate on the boundary where the material is drawn into the control volume domain is expected to be 0·0025 m/s due to incompressibility. This was found to be satisfied well. The velocity distributions shown in Figure 4 for the centerline and for the surface of the workpiece are both found to be close to the value that would be obtained for a slab flow. This is a reasonable result for this case with low friction and low die angle.

In this work, the sensitivity of the required power and of the internal state variable to the die shape are being examined. To demonstrate the effect of the die shape on these quantities, the results for four typical die shapes are presented. The four die shapes considered are straight, concave, convex and sigmoidal and these are shown in Figure 5. The power required for each of

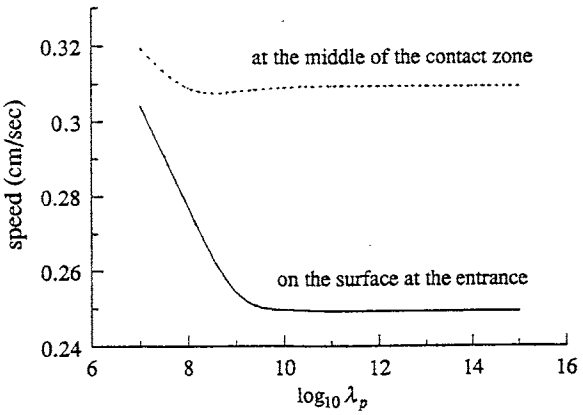

Figure 2. Effect of the penalty parameter on the computed velocities

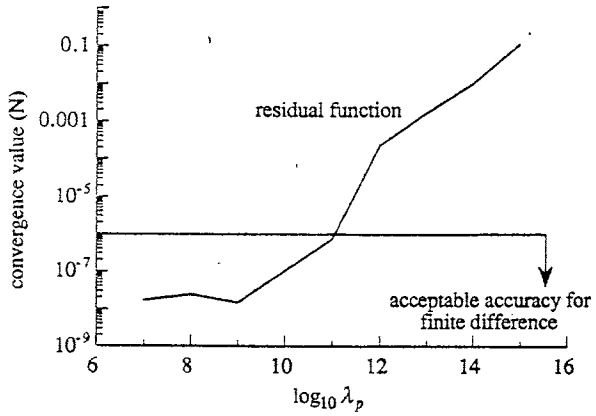

Figure 3. Effect of the penalty parameter on the converged value of the residual function

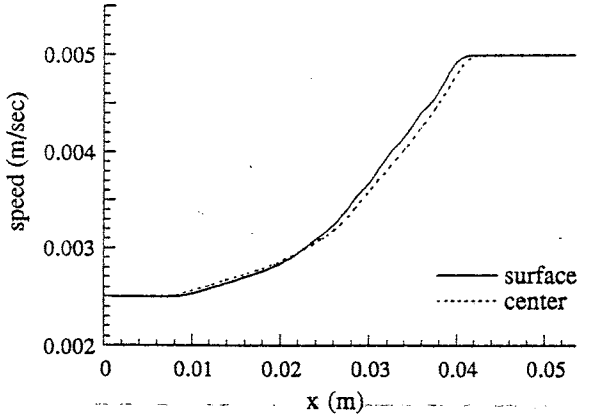

Figure 4. Speed distribution for the workpiece along the surface and at the centerline

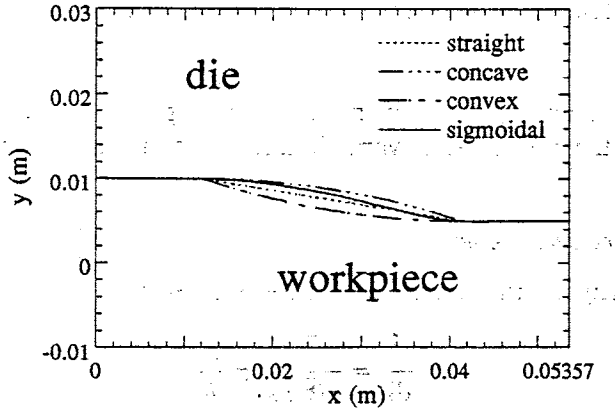

Figure 5. Example die shapes

these die shapes is plotted in Figure 6. For this example, the convex die is shown to have the greatest power requirement while the straight die is found to have the lowest power requirement and there is a significant difference between these. The state variable distributions through the

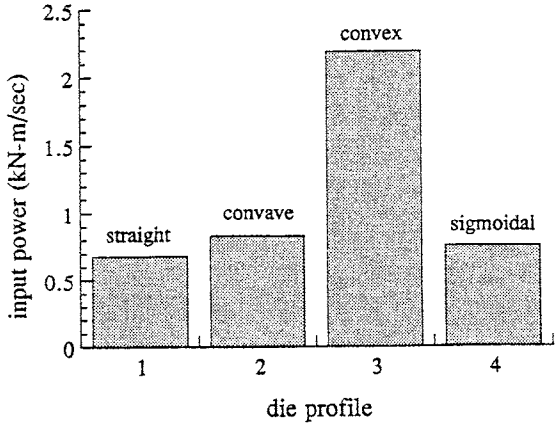

Figure 6. Power requirement for various die shapes

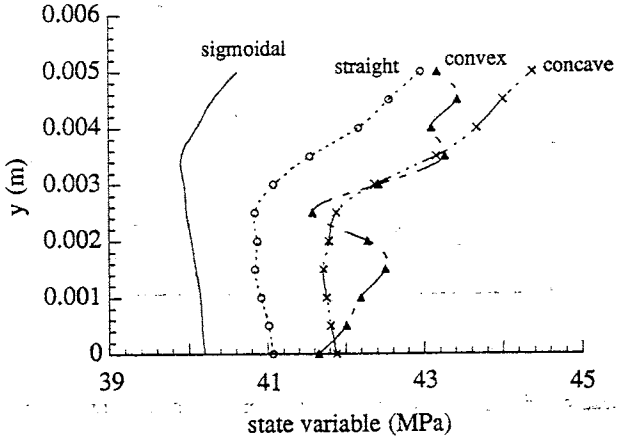

Figure 7. State variable distribution through the thickness for various die shapes

thickness in the exit are shown for the four die shapes in Figure 7. It is clear to see that the die shape has an effect on the internal state variable distribution in the final product.

4.2. Experiment II: Force sensitivities

Let the force sensitivity matrix be defined in dimensionless form as

$$\tilde{\mathbf{B}} = \frac{\mathrm{d}\tilde{\mathbf{f}}'}{\mathrm{d}\tilde{\mathbf{b}}} = \frac{\mathrm{d}(\bar{\mathbf{f}}'/f_0)}{\mathrm{d}(\bar{\mathbf{b}}/b_0)} = \frac{b_0}{f_0}\mathbf{B}$$

where b_0 is the thickness of the strip in the entrance (in this example, 0·01 m), f_0 is the order of the initial input force (in this case, 10^5 N), and $\tilde{\mathbf{f}}'$ and $\tilde{\mathbf{b}}$ are the normalized vectors of $\bar{\mathbf{f}}'$ and $\bar{\mathbf{b}}$, respectively. Equation (17) is a complicated expression for $\mathbf{B}$. Therefore, it is desirable to investigate if a simplified approximate form can be found that may save computational time. This can be accomplished by observing that in many cases, the matrices $\mathbf{K}_s$ and $\mathbf{H}_u$ are very small

compared to the other matrices. If these terms are neglected, the force sensitivity matrix is significantly reduced to

$$\tilde{\mathbf{B}}_s = \frac{b_0}{f_0}\left[\mathbf{K}_b^* + \mathbf{K}_u^*(\mathbf{K}_u)^{-1}(\mathbf{F}_b - \mathbf{K}_b)\right]$$

where $\tilde{\mathbf{B}}_s$ is the simplified dimensionless force sensitivity matrix. Computing the sensitivity matrix using this simplified form will be referred to as the simplified adjoint method.

Consider the case with 14 design variables which consist of the y-co-ordinates of the nodes on $\partial\hat{B}$ (the co-ordinate of the node common to boundaries $\partial\hat{B}$ and ∂B^f is taken to be fixed and the co-ordinate of the node common to boundaries $\partial\hat{B}$ and $\partial\tilde{B}$ is variable). The vector $\tilde{\mathbf{b}}$ is used to represent the normalized values of the y-co-ordinates of the nodes on $\partial\hat{B}$ in the following results (Figures 8–11). The die shape is the same as shown in Figure 1. Figures 8 and 9 show the resulting force sensitivities for different nodes on which the load is applied and for different design shape parameters, respectively. Results from the Adjoint Method (AM), the Simplified Adjoint Method (SAM) and the Finite Difference method (FD), i.e. using equation (7), are in good agreement. Differences between these methods result from the finite difference approximations used in computing some of the derivatives.

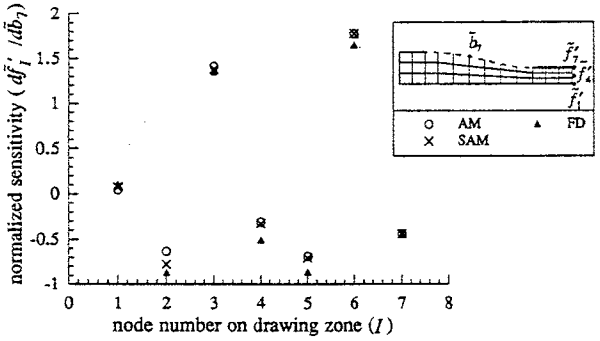

Figure 8. Sensitivity parameters, $\tilde{B}_{I7}$, $I = 1, 7$, where I is the node number on the drawing zone. Compares results for the AM, SAM and the Finite Difference FD method

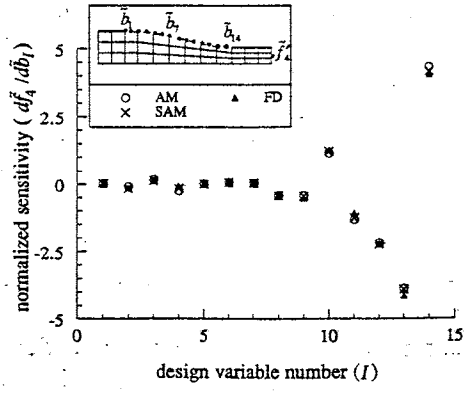

Figure 9. Sensitivity parameters $\tilde{B}_{4I}$, $I = 1, 14$, where I is the design variable number. Compares results for the AM, SAM and the FD method

The computational time for the sensitivity analysis is on the same order as that for solving the direct problem. Specifically in the presented example, the CPU time on a Sun SPARC-10 Model 30 is 58·30 sec for solving the direct problem. For the sensitivity analysis, the CPU time is 95·68 sec by the adjoint method, 84·59 sec by the simplified adjoint method and 381·46 sec by the finite difference approach. It should be noted that in determining the sensitivity parameters it is necessary first to solve the direct problem about which the sensitivity parameters are determined (step (1) in the procedure given above). The times listed above for the sensitivity analysis include the time to solve the direct problem. If this is subtracted out, the time that is left is the time it takes to compute the sensitivity parameters for a given $\bar{\mathbf{u}}$ and $\bar{\mathbf{s}}$ (steps (2)–(6)) in the above procedure. For the adjoint method, this is only 37·38 sec and for the simplified adjoint method, it is 26·29 sec. The adjoint method for the sensitivity analysis is very efficient and becomes crucial for problems with a refined mesh or for more complicated forming processes.

4.3. *Experiment III: Internal state variable sensitivities*

The internal state variable sensitivity matrix can be defined in dimensionless form as

$$\tilde{\mathbf{C}} = \frac{\mathrm{d}\tilde{\mathbf{s}}'}{\mathrm{d}\tilde{\mathbf{b}}} = \frac{\mathrm{d}(\bar{\mathbf{s}}'/s_0)}{\mathrm{d}(\bar{\mathbf{b}}/b_0)} = \frac{b_0}{s_0}\mathbf{C}$$

where s_0 is the initial internal state variable of the material and $\tilde{\mathbf{s}}'$ is the normalized vector of $\bar{\mathbf{s}}'$. Figures 10 and 11 show the resulting internal state variable sensitivities. These results are for the nodes on which the workpiece is drawn out of the domain and different design shape parameters, respectively. Results from the adjoint method and the finite difference approach are in good agreement. As in the previous case, the computation by the adjoint method is quite efficient. In fact, the matrix $\mathbf{C}$ is needed for the computation of $\mathbf{B}$ as can be seen by comparing equations (17) and (18).

4.4. *Discussion*

The resulting sensitivities in Figures 8 through 11 show the significance of the forming-process geometry to the input force and the internal state variable. The input force relates to the manufacturing cost. The internal state variable in general relates to the material properties, such as grain size, hardness and strength (see Reference 19 for details of the model used herein). The optimization of the process geometry is a process design problem and is referred to as shape optimization. In process design problems, the sensitivities provide important information for the optimization algorithm which is often based on a gradient method for minimizing an objective function. In highly non-linear problems, such as the one considered in this paper, verifying the accuracy of the numerically computed sensitivities becomes especially important. The accuracy of the sensitivities computed in equations (17) and (18) depends on the accuracy of the convergence of the system equations (as shown in Figure 3) because of the finite difference approximation for $\mathbf{K}_b$, $\mathbf{F}_b$ and $\mathbf{H}_b$. Our numerical experience indicates that the numerical study of the forward problem and the convergence study carried out in Experiment I is useful for a confident sensitivity analysis based on the presented formulation. In addition, the tool shape (design curve) should be accurately interpolated for computing the first-order shape derivatives such that the finite difference approximation produces little computational error in equations (17) and (18). This is because the boundary conditions on $\partial\hat{B}$ depend on tangent directions which will in turn depend on the interpolation of the tool shape.

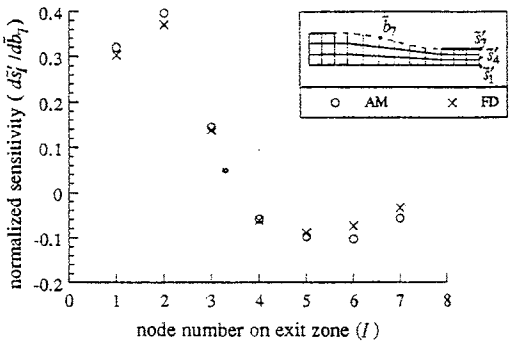

Figure 10. Sensitivity parameters , $\bar{C}_{I7}$, $I = 1, 7$, where I is the node number on the exit zone. Compares results for the AM and the FD method

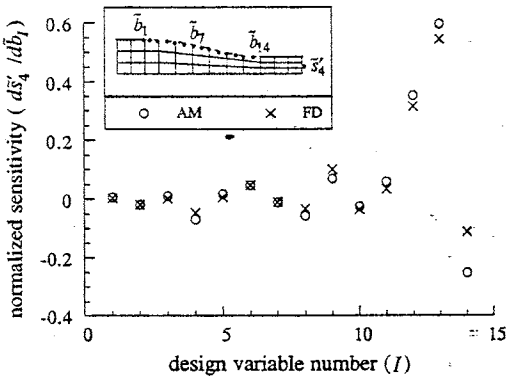

Figure 11. Sensitivity parameters $\bar{C}_{4I}$, $I = 1, 14$, where I is the design variable number. Compares results for the AM and the FD method

5. CONCLUSION

Numerical algorithms for computing shape sensitivity parameters for specific applications in steady-state metal forming have been presented. The adjoint method and in the case of force sensitivities, a simplified adjoint method, have been found to be efficient and to give acceptably accurate results.

In future work, the algorithms for computing the sensitivity parameters derived herein will be incorporated into global optimization and inverse algorithms for optimizing process geometries in steady metal-forming applications. Preliminary test cases in this area performed by the authors have shown promise. More complex geometries and thermal effects will be considered in the future. Eventually, when the model is found to be sufficiently realistic, experimental dies with predicted die shapes will be fabricated and tested.

ACKNOWLEDGEMENTS

This work was supported by the Henry Luce Foundation, Inc. and by the National Science Foundation through Grant DMI-9358123.

APPENDIX I

The two-dimensional steady forming problem described in this study is discretized by the finite element formulation. The kinematic equations are expressed in the form

$$\bar{\mathbf{k}}(\bar{\mathbf{u}}, \bar{\mathbf{s}}) = (\bar{\mathbf{K}} + \overline{\mathbf{GM}}^{-1}\bar{\mathbf{G}}^{\mathrm{T}})\bar{\mathbf{u}} = \bar{\mathbf{f}}$$

and the constitutive equations

$$\bar{\mathbf{h}}(\bar{\mathbf{u}}, \bar{\mathbf{s}}) = \mathbf{0}$$

where

$$u_i = \bar{u}_{i\alpha}\psi_\alpha, \quad i = 1, 2 \quad \alpha = 1, n_u$$

$$s = \bar{s}_\alpha \psi_\alpha, \quad \alpha = 1, n_u$$

$$p = \bar{p}_\gamma \tilde{\psi}_\gamma, \quad \gamma = 1, n_p$$

$$\bar{\mathbf{K}} = \sum_{m=1}^{M} K^m_{j\beta i\alpha}, \quad K^m_{j\beta i\alpha} = \int_{B_m} \mu_e(\delta_{ij}\psi^m_{\alpha,k}\psi^m_{\beta,k} + \psi^m_{\alpha,j}\psi^m_{\beta,i})\,\mathrm{d}V$$

$$\bar{\mathbf{G}} = \sum_{m=1}^{M} G^m_{j\beta\gamma}, \quad G^m_{j\beta\gamma} = \int_{B_m} \psi^m_{\beta,j}\tilde{\psi}^m_\gamma \mathrm{d}V$$

$$\bar{\mathbf{M}} = \sum_{m=1}^{M}, M^m_{\zeta\gamma}, \quad M^m_{\zeta\gamma} = \frac{1}{\lambda_p}\int_{B_m} \psi^m_\zeta \tilde{\psi}^m_\gamma \,\mathrm{d}V$$

$$\bar{\mathbf{f}} = \sum_{m_s=1}^{M} \bar{f}^{m_s}_{j\beta}, \quad \bar{f}^{m_s}_{j\beta} = \int_{\partial B_{m_s}} t_j \psi^{m_s}_\beta \,\mathrm{d}S$$

$$\bar{\mathbf{h}} = \sum_{m=1}^{M} \bar{h}^m_\gamma, \quad \bar{h}^m_\gamma = \int_{B_m} [\bar{s}_\alpha \psi^m_{\alpha,i}\bar{u}_{i\beta}\psi^m_\beta - g(\dot{\varepsilon}, s)]\,\psi^m_\gamma \,\mathrm{d}V$$

The plane domain B is divided into M finite elements of area B_m, $m = 1, M$; M_s is the number of surface elements; ψ^m_α is an element shape function for interpolating the velocity field; $\tilde{\psi}^m_\gamma$ is an element shape function for interpolating the pressure field; n_u and n_p are the number of nodes per element used in the velocity and pressure interpolations, respectively; λ_p is a penalty parameter for imposing the incompressibility constraint; and the evolution function $g(\dot{\varepsilon}, s)$ used herein is shown in Table I. In addition, repeated indices indicate summation, the Greek subscripts denote node numbers and the Roman subscripts denote nodal degrees of freedom.

APPENDIX II

The derivatives in equations (17) and (18) are computed as follows:

(1) $\mathbf{K}_u$ matrix

$$\mathbf{K}_u = \bar{\mathbf{K}} + \overline{\mathbf{GM}}^{-1}\bar{\mathbf{G}}^{\mathrm{T}} + \bar{\mathbf{K}}_T$$

where

$$\bar{\mathbf{K}}_T = \sum_{m=1}^{M} K^m_{T_{j\beta i\alpha}}, \quad K^m_{T_{j\beta i\alpha}} = \int_{B_m} \frac{4}{3\dot{\varepsilon}} \frac{\partial \mu_e}{\partial \dot{\varepsilon}} D_{il} \psi^m_{\alpha,l} D_{jk} \psi^m_{\beta,k} \, dV$$

(2) $\mathbf{K}_s$ matrix

$$\mathbf{K}_s = \sum_{m=1}^{M} K^m_{s_{j\beta\alpha}}, \quad K^m_{s_{j\beta\alpha}} = \int_{B_m} 2 \frac{\partial \mu_e}{\partial s} D_{ij} \psi^m_{\alpha,l} \psi^m_{\beta,i} \, dV$$

(3) $\mathbf{H}_s$ matrix

$$\mathbf{H}_s = \sum_{m=1}^{M} H^m_{s_{\gamma\alpha}}, \quad H^m_{s_{\gamma\alpha}} = \int_{B_m} [\psi^m_{\alpha,i} \bar{u}_{i\beta} \psi^m_\beta - \frac{\partial g}{\partial s} \psi^m_\alpha] \psi^m_\gamma \, dV$$

(4) $\mathbf{H}_u$ matrix

$$\mathbf{H}_u = \sum_{m=1}^{M} H^m_{u_{\gamma i\alpha}}, \quad H^m_{u_{\gamma i\alpha}} = \int_{B_m} [\bar{s}_\beta \psi^m_{\beta,i} \psi^m_\alpha - \frac{2}{3\dot{\varepsilon}} \frac{\partial g}{\partial \dot{\varepsilon}} D_{ij} \psi^m_{\alpha,j}] \psi^m_{\alpha,j} \, dV$$

APPENDIX III

Notation

The following notation is used throughout this paper. Vectors denoting field variables, such as velocity, are expressed in lower case bold, for example **u**, and tensors are denoted with upper case bold, for example **T**. Scalar quantities or components of vectors and tensors are in italics, for example, $\hat{u}_i$. Vectors of nodal point quantities (column matrices), for example the velocities at the finite element nodes, are denoted in lower case bold with an overbar, for example $\bar{\mathbf{u}}$. Matrices are denoted in upper case bold and are clearly indicated as matrices in the text to differentiate from tensors. The operator tr( ) is the trace operator, div( ) is the divergence operator and ∇( ) is the gradient operator. The inner product is always denoted by a dot ($\cdot$). For vectors, the inner product is written as $\mathbf{u} \cdot \mathbf{v}$ and is defined in component form as $u_i v_i$ where summation is implied on repeated indices. For tensors, the inner product is defined as $\mathbf{A} \cdot \mathbf{B} \equiv (\mathbf{A}^T \mathbf{B})$ where superscript T denotes the transpose. Lower case Roman subscripts indicate degree of freedom (co-ordinate direction), lower case Greek subscripts indicate node number, and upper case Roman subscripts indicate the position in a matrix. In addition, the following symbols are used in this paper.

$\bar{\mathbf{b}}, \tilde{\mathbf{b}}$	vector of shape design parameters in dimensional and dimensionless forms
B	domain of interest
∂B	boundary of B
$\partial B_s, \partial B_e$	boundaries on the entrance and on the exit of the domain
$\partial B', \partial \hat{B}$	boundary on which the load is applied, boundary on the tool contact zone
$\partial B_{1i}, \partial B_{2i}, \partial B_{3i}$	boundaries with velocity, traction and friction boundary conditions

∂B^f, $\partial \tilde{B}$	boundary with a free surface, boundary with zero traction in the x-direction and zero velocity in the y-direction
$\mathbf{B}$, $\mathbf{C}$	shape sensitivity matrices
$\tilde{\mathbf{B}}$, $\tilde{\mathbf{C}}$	dimensionless shape sensitivity matrices
$\tilde{\mathbf{B}}_s$	simplified approximation of $\tilde{\mathbf{B}}$
$\mathbf{D}$	rate of deformation tensor
$\bar{\mathbf{f}}$, $\bar{\mathbf{f}}'$	nodal force vector, part of nodal force vector acting on $\partial B'$
$\tilde{\mathbf{f}}'$	dimensionless form of $\bar{\mathbf{f}}'$
$\bar{\mathbf{f}}^*$	nodal force vector for system with no boundary condition prescribed on $\partial B'$
$\mathbf{F}_b$, $\mathbf{H}_b$, $\mathbf{H}_u$, $\mathbf{H}_s$, $\mathbf{K}_b$, $\mathbf{K}_s$, $\mathbf{K}_b^*$, $\mathbf{K}_u^*$, $\mathbf{K}_s^*$	matrices of derivatives as defined in Section 3.1
$\bar{\mathbf{h}}$	discretized state variable evolution equation
$\bar{\mathbf{k}}$, $\bar{\mathbf{k}}^*$	left-hand side of discretized weak form of the equilibrium equation with and without a boundary condition prescribed on $\partial B'$
L, $\tilde{L}$	augment Lagrangians used in computing $\mathbf{B}$ and $\mathbf{C}$
$\mathbf{n}$	unit outward normal on B
N	total number of nodes for the velocity interpolation
N_d	number of shape design parameters
$N_{B'}$	number of nodes on the boundary with the applied load $\partial B'$
N_{B_e}	number of nodes on the exit boundary ∂B_e
p	pressure
P	power required to perform the deformation process
$\bar{\mathbf{q}}$, $\bar{\mathbf{r}}$	vectors of general functions for which the sensitivities are to be determined
$\mathbf{Q}$, $\mathbf{R}$	rectangular matrices for extracting desired components of the sensitivity matrices
s, $\hat{s}$	internal state variable field and its value prescribed on ∂B_s
$\bar{\mathbf{s}}$, $\bar{\mathbf{u}}$	vectors of nodal state variables and nodal velocities
$\bar{\mathbf{s}}'$, $\tilde{\mathbf{s}}'$	vectors of nodal state variables on ∂B_e in dimensional and dimensionless forms
$\bar{\mathbf{s}}^a$, $\bar{\mathbf{u}}^a$	vectors of admissible adjoint variables
$\mathbf{t}$	traction
$\hat{t}_i$, $\hat{u}_i$	prescribed components of the tractions and velocities on boundaries ∂B_{1i} and ∂B_{2i}
$\hat{\mathbf{t}}$, $\bar{\mathbf{t}}'$	vectors of nodal tractions on ∂B_{2i} and $\partial B'$
$\mathbf{T}$, $\mathbf{T}'$	Cauchy stress tensor and deviatoric Cauchy stress tensor
$\mathbf{u}$	velocity
$\mathbf{u}'$, $\bar{\mathbf{u}}'$	tool velocity on $\partial B'$ where the load is applied for performing the deformation and nodal velocities on $\partial B'$
W_1^a, W_2^a	state equations used for forming augmented Lagrangians
β	coefficient in relative velocity friction law
$\dot{\varepsilon}$	effective rate of deformation ($\sqrt{\frac{2}{3}\,\mathbf{D}\cdot\mathbf{D}}$)
σ	effective stress ($\sqrt{\frac{3}{2}\,\mathbf{T}'\cdot\mathbf{T}'}$)

λ_p penalty parameter used to enforce the incompressibility
μ_e effective viscosity
$\varphi_\alpha, \psi_\alpha^m, \tilde{\psi}_\gamma^m$ shape functions

REFERENCES

1. P. R. Dawson, 'On modeling of mechanical property changes during flat rolling of aluminum', *Int. J. Solids Struct.*, **23**, 947–968 (1987).
2. A. M. Maniatty, 'Predicting residual stresses in steady forming processes', *Comp. Sys. Eng.*, **5**, 171–177 (1994).
3. G. Weber and L. Anand, 'Finite deformation constitutive equations and a time integration procedure for isotropic, hyperelastic–viscoplastic solids', *Comp. Methods. Appl. Mech. Eng.*, **79**, 173–202 (1990).
4. S. Kobayashi, S. Oh and T. Altan, *Metal Forming and the Finite Element Method*, Oxford University Press, New York, 1989.
5. J. Haslinger and P. Neittaanmaki, *Finite Element Approximation for Optimal Shape Design Theory and Application*, Wiley, New York, 1988.
6. S. Y. Jao and J. S. Arora, 'Design optimization of non-linear structures with rate-dependent and rate-independent constitutive models', *Int. j. numer. methods eng.*, **36**, 2805–2834 (1993).
7. A. M. Maniatty and N. J. Zabaras, 'Investigation of regularization parameters and error estimating in inverse elasticity problems', *Int. j. numer. methods. eng.*, **37**, 1039–1052 (1994).
8. M. L. Wenner, 'Elementary solutions and process sensitivities for plane-strain sheet-metal forming', *J. Appl. Mech.*, **59**, 23–28 (1992).
9. G. Maccarini, C. Giardini, G. Pellegrini and A. Bugini, 'The influence of die geometry on cold extrusion forging operations: FEM and experimental results', *J. Mater. Process. Technol.*, **27**, 227–238 (1991).
10. S. Aizicovici and N. S. Papageorgiou, 'A sensitivity analysis of Volterra integral inclusions with applications to optimal control problems', *J. Math. Anal. Appl.*, **186**, 97–119 (1994).
11. J. M. House, J. S. Arora and T. F. Smith, 'Comparison of methods for design sensitivity analysis for optimal control of thermal systems', *Opt. Control Appl. Methods*, **14**, 17–37 (1993).
12. T. C. Lin and J. S. Arora, 'Differential dynamic programming technique for optimal control', *Opt. Control Appl. Methods*, **15**, 77–100 (1994).
13. D. A. Tortorelli, 'Sensitivity analysis for non-linear constrained elastostatic systems', *Int. j. numer. methods eng.*, **33**, 1643–1660 (1992).
14. J. S. Arora and J. B. Cardoso, 'Variational principle for shape design sensitivity analysis', *AIAA J.*, **30**, 538–547 (1992).
15. J. J. Tsay and J. S. Arora, 'Non-linear structural design sensitivity analysis for path-dependent problems, part 1: general theory', *Comp. Methods Appl. Mech. Eng.*, **81**, 183–208 (1990).
16. J. J. Tsay, J. B. Cardoso and J. S. Arora, 'Non-linear structural design sensitivity analysis for path-dependent problems, part 2: analytical example problems', *Comp. Methods Appl. Mech. Eng.*, **81**, 209–228 (1990).
17. O. Zhang, S. Mukherjee and A. Chandra, 'Design sensitivity coefficients for elasto-viscoplastic problems by boundary element methods', *Int. j. numer. methods eng.*, **34**, 947–966 (1992).
18. P. Michaleris, D. A. Tortorelli and C. A. Vidal, 'Tangent operators and design sensitivity formulations for transient non-linear coupled problems with applications to elastoplasticity', *Int. j. numer. methods eng.*, **37**, 2471–2499 (1994).
19. S. B. Brown, K. H. Kim and L. Anand, 'An internal variable constitutive model for hot working of metals', *Int. J. Plasticity*, **5**, 95–130 (1989).
20. M. S. Engelman, R. L. Sani, P. M. Gresho and M. Bercovier, 'Consistent versus reduced integration penalty methods for incompressible media using several old and new elements', *Int. j. numer. methods fluids*, **2**, 25–42 (1982).
21. O. C. Zienkiewicz, R. L. Taylor and J. M. Too, 'Reduced integration technique in general analysis of plates and shells', *Int. j. numer. methods eng.*, **3**, 275–290 (1971).
22. J. T. Oden, 'Penalty method and reduced integration for the analysis of fluids', in J. N. Reddy (ed.), *Penalty Finite Element Methods in Mechanics*, ASME, New York, 1982, pp. 21–32.
23. T. J. R. Hughes, *The Finite Element Method: Linear Static and Dynamic Finite Element Analysis*, Prentice-Hall, Englewood, Cliffs, N.J., 1987.
24. M. D. Gunzburger and R. A. Nicolaides, *Incompressible Computational Fluid Dynamics: Trends and Advances*, Cambridge University Press, New York, 1993.
25. F. Brezzi and M. Fortin, *Mixed and Hybrid Finite Element Methods*, Springer-Verlag, New York, 1991.
26. R. T. Haftka, 'Semi-analytical static non-linear structural sensitivity analysis', *AIAA J.*, **31**, 1307–1312 (1993).